JACS
JOURNAL OF THE AMERICAN CHEMICAL SOCIETY

ARTICLE

pubs.acs.org/JACS

Large-Scale Synthesis of Bioinert Tantalum Oxide Nanoparticles for X-ray Computed Tomography Imaging and Bimodal Image-Guided Sentinel Lymph Node Mapping

Myoung Hwan Oh,[†,∥] Nohyun Lee,[†,∥] Hyoungsu Kim,[‡] Seung Pyo Park,[†] Yuanzhe Piao,[§] Jisoo Lee,[†] Samuel Woojoo Jun,[†] Woo Kyung Moon,[‡] Seung Hong Choi,[*,‡] and Taeghwan Hyeon[*,†]

[†]National Creative Research Initiative Center for Oxide Nanocrystalline Materials, World Class University (WCU) Program of Chemical Convergence for Energy & Environment (C_2E_2), and School of Chemical and Biological Engineering, Seoul National University, Seoul 151-744, Korea

[‡]Radiology, Seoul National University Hospital, and the Institute of Radiation Medicine, Medical Research Center, Seoul National University, 28, Yeongeon-dong, Jongno-gu, Seoul 110-744, Korea

[§]Department of Nano Science and Technology, Graduate School of Convergence Science and Technology, Seoul National University, Suwon 443-270, Korea

Supporting Information

ABSTRACT: Ever since Au nanoparticles were developed as X-ray contrast agents, researchers have actively sought alternative nanoparticle-based imaging probes that are not only inexpensive but also safe for clinical use. Herein, we demonstrate that bioinert tantalum oxide nanoparticles are suitable nanoprobes for high-performance X-ray computed tomography (CT) imaging while simultaneously being cost-effective and meeting the criteria as a biomedical platform. Uniformly sized tantalum oxide nanoparticles were prepared using a microemulsion method, and their surfaces were readily modified using various silane derivatives through simple in situ sol−gel reaction. The silane-modified surface enabled facile immobilization of functional moieties such as polyethylene glycol (PEG) and fluorescent dye. PEG was introduced to endow the nanoparticles with biocompatibility and antifouling activity, whereas immobilized fluorescent dye molecules enabled simultaneous fluorescence imaging as well as X-ray CT imaging. The resulting nanoparticles exhibited remarkable performances in the in vivo X-ray CT angiography and bimodal image-guided lymph node mapping. We also performed an extensive study on in vivo toxicity of tantalum oxide nanoparticles, revealing that the nanoparticles did not affect normal functioning of organs.

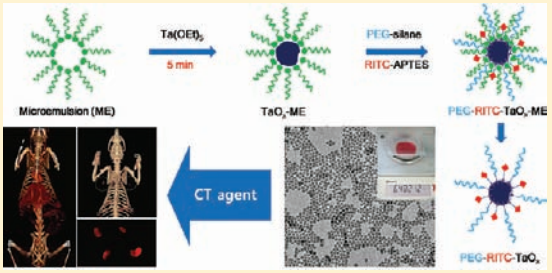

INTRODUCTION

Colloidal nanoparticles have been intensively investigated for their biomedical applications related to imaging, diagnostics, and therapeutics due to their unique electronic, optical, and magnetic properties.[1] Injected nanoparticles can evade phagocytosis of reticuloendothelial system (RES) and accumulate in targeted organs. Circulation time and interactions with various cells such as macrophages are highly dependent on the size and surface properties of nanoparticles. Consequently, there have been extensive efforts to develop effective nanobiomedical platforms based on inorganic nanoparticles.[2] For example, semiconductor nanoparticles, also known as quantum dots (QDs), have been extensively studied as fluorescent probes for optical imaging.[3] On the other hand, magnetic nanoparticles have been used as contrast agents in magnetic resonance imaging (MRI).[4]

X-ray computed tomography (CT) is one of the most popular diagnostic imaging techniques in clinical use, due to its merits such as cost effectiveness, high-contrast resolution, unlimited penetration depth, and facile image processing.[5] However, for accurate diagnosis, administration of a large amount of contrast agent is often required because sensitivity and soft tissue contrast are inherently low in X-ray CT imaging. Therefore, cost should be seriously considered in the design of new X-ray CT contrast agents.[6a,b] Currently, iodinated compounds are widely used as CT contrast agents with an emphasis on its cost-effectiveness and safety than its performance. However, small iodinated compounds are rapidly excreted via renal elimination, resulting in short circulation time that limits their applications for target-specific imaging and angiography.[6]

Recently, various nanoparticles have been introduced as potential candidates for X-ray contrast agents.[7] As compared to conventional iodine-based contrast agents, nanoparticle-based agents are characterized by superior contrast enhancement and prolonged blood circulation time. Furthermore, nanoparticles can be easily functionalized with various biomolecules for tissue-specific

Received: January 5, 2011
Published: March 23, 2011

uptake and multimodal imaging applications, resulting in more dependable diagnostic information.[8] However, dissolution or aggregation of the nanoparticles in blood vessels can cause severe toxicity or fatal embolism, respectively, and it can become even more serious when large dose is used during X-ray CT imaging. Therefore, colloidal stability of the nanoparticles has been the most important issue for their clinical applications. This requirement is also closely related to the surface chemistry of the nanoparticles. Consequently, the development of inexpensive and nontoxic nanoparticles with facile and reliable surface modification capability is highly desirable.

Until now, the most studied nanomaterials for X-ray contrast agents are nanoparticles of Au and Bi_2S_3.[7] Bi_2S_3 nanoparticles have apparent limitations due to the intrinsic toxicity of Bi. Although it is relatively easy to synthesize and functionalize Au nanoparticles, the cost of using gold as X-ray contrast agent is a huge obstacle to their clinical utilization. Tantalum is another strong candidate as a CT contrast agent due to its high X-ray attenuation coefficient and bioinertness.[9] Because of their relative nontoxicity, tantalum and tantalum oxide have been widely used in clinical applications as a part of radiographic markers, implants, artificial joints, stents, and vascular clips.[9] Moreover, tantalum is much cheaper than gold while possessing a comparable X-ray attenuation coefficient (Ta, 4.3 and Au, 5.16 cm^2/kg at 100 eV). Recently, water-soluble sub-10 nm tantalum oxide nanoparticles were synthesized for X-ray/CT imaging applications.[10] Although X-ray contrast was enhanced by the tantalum oxide nanoparticles, rapid renal clearance occurred. While rapid clearance of nanoparticles is desirable in some cases, the limited image acquisition time should be problematic for applications other than angiography. Herein, we report facile and large-scale synthesis of uniform-sized tantalum oxide (TaO_x) nanoparticles via microemulsion method under ambient conditions. The surface of the TaO_x nanoparticles was easily modified by silane derivatives. Surface modification with fluorophore or polymer allowed the nanoparticles to be successfully used as an in vivo X-ray CT contrast agent for angiography and bimodal image-guided lymph node mapping.[11] For the first time, in vivo toxicity of tantalum oxide nanoparticles was systematically examined. It was found that the nanoparticles did not cause any significant adverse effect on liver and other organs.

EXPERIMENTAL SECTION

Synthesis of TaO_x Nanoparticles in Microemulsion. Microemulsion (ME) was prepared by adding 0.25 mL of NaOH aqueous solution (75 mM) to the oil phase composed of 2.3 g of Igepal CO-520 (Aldrich), ethanol (Samchun, 99.5%), and 20 mL of cyclohexane (Samchun, 99.5%). After 0.05 mL of tantalum(V) ethoxide (0.3 mmol, Strem, 99.8%) was added to the ME at room temperature, a resulting mixture containing tantalum oxide nanoparticles (designated as TaO_x-ME) was synthesized within 5 min. To control the size of the TaO_x nanoparticles, the amount of ethanol was varied (0, 0.25, 0.5, and 0.75 mL).

One-Pot Surface Modification of TaO_x Nanoparticles: Pegylation and Rhodamine-B-isothiocyanate (RITC) Functionalization of TaO_x Nanoparticles for Bimodal Imaging Applications. To prepare rhodamine-B-isothiocyanate (RITC)-functionalized silane, 110 μL of aminopropyltriethoxysilane (APTES, Aldrich) was reacted with 50 mg of RITC in 3.75 mL of ethanol at room temperature for 24 h. The resulting solution along with 12.5 mL of 2-methoxy(polyethyleneoxy)propyltrimethoxysilane (PEG-silane, Gelest, 596−725 Da) was added to 1 L of the as-prepared TaO_x-ME. The mixture was then stirred at room temperature for 24 h, becoming a red turbid solution. The resulting solution was evaporated at 60 °C until the solution became transparent, after which the functionalized TaO_x nanoparticles were precipitated by adding a mixed solution of 1:1 (v/v) ether/*n*-hexane. The precipitates were purified with ether and dispersed in ethanol. To this solution was added 100 mg of methoxypoly(ethylene glycol) succinimidylglutarate (mPEG-SG, MW 2000, Sunbio). The mixture was stirred overnight at 30 °C to conjugate PEG onto residual amine groups on the surface of the functionalized TaO_x nanoparticles. After being washed several times with deionized water, the final product, designated as PEG-RITC-TaO_x, was dispersed in phosphate buffered saline (PBS) buffer.

X-ray CT and Fluorescence Imaging with PEG-RITC-TaO_x. *Phantom Test.* Various concentrations of PEG-RITC-TaO_x (0.22, 0.45, 0.9, 1.8, 3.6, 7.2, 14.5, and 29 mg of Ta/mL) dispersed in deionized water were prepared in 1.5 mL microtubes. CT images were acquired using a dual-source CT system (Somatom Definition, Simens). Imaging parameters were as follows: thickness, 1 mm; pitch, 1; 120 kVp, 90 mA; field of view, 84 × 84; gantry rotation time, 0.5 s; table speed, 6 mm/s.

Cell Culture. RAW264.7 (murine macrophage cell line) was grown in monolayers in Dulbecco's Modified Eagle's Medium (DMEM, WelGENE) supplemented with 10% (v/v) fetal bovine serum (FBS, Gibco) and penicillin/streptomycin (100 U/mL and 100 μg/mL, respectively, Gibco) in a humidified 5% CO_2 atmosphere at 37 °C.

Cellular Uptake. To observe cellular uptake of the TaO_x nanoparticles, 1×10^4 RAW 264.7 cells per well were cultured in an 8-well chamber slide (NalgenNunc, Naperville, IL) and incubated with PEG-RITC-TaO_x at various concentrations (0, 0.6, 1.2, and 2.4 mg of Ta/mL). After 24 h, the cells were washed with PBS, fixed with 4% paraformaldehyde, and stained with 4′,6-diamidino-2-phenylindole (DAPI, 1 μg/mL in PBS, Roche). Fluorescence images were acquired by confocal laser scanning microscopy (CLSM) (LSM 510, Carl Zeiss, Germany).

Cell Viability Assay. The viability and proliferation of cells in the presence of TaO_x nanoparticles were evaluated by 3-[4,5-dimethylthiazol-2-yl]-2,5-diphenyltetrazolium bromide (MTT, Sigma) assay. The assay was performed in triplicate in the following manner. RAW264.7 cells were seeded into 96-well plates at a density of 1×10^4 cells per well in 200 μL of media and grown overnight. The cells were then incubated with various concentrations of PEG-RITC-TaO_x (0, 0.075, 0.15, 0.3, 0.6, 1.2, and 2.4 mg of Ta/mL) for 24 h. Following incubation, cells were incubated in media containing 0.1 mg/mL of MTT for 1 h. Thereafter, MTT solution was removed, and precipitated violet crystals were dissolved in 200 μL of DMSO. The absorbance was measured at 560 nm using a VersaMax microplate reader (Molecular Devices).

In Vitro CT Imaging. RAW264.7 cells were seeded onto culture dishes at a density of 1×10^6 cells per plate in 10 mL of media and grown overnight. Subsequently, various concentrations of PEG-RITC-TaO_x (0, 0.63, 1.3, and 2.5 mg of Ta/mL) dispersion were added. After 24 h, the cells were washed twice with PBS to remove free nanoparticles and detached by the addition of 1 mL of trypsin/EDTA (Gibco). After centrifugation at 1500 rpm for 5 min, cells were dispersed in 1 mL of culture media and transferred to a 1.5 mL microtube. Cell pellets were prepared by centrifugation at 2000 rpm for 5 min. CT images were acquired using a dual-source CT system (Somatom Definition, Simens). Imaging parameters were as follows: thickness, 1 mm; pitch, 1; 120 kVp, 90 mA; field of view, 84 × 84; gantry rotation time, 0.5 s; table speed, 6 mm/s.

In Vivo CT Imaging. CT images were acquired prior to injection of PEG-RITC-TaO_x as well as at appropriate time points after administration. Rats were anesthetized by intraperitoneal injection of a mixture of Zoletil (1.92 mg/kg; Virbac, France), Rompun (0.48 mg/kg; Bayer Korea, Korea), and saline. Next, 1 mL of PEG-RITC-TaO_x dispersion (840 mg/kg) was injected through the tail vein of the rat. For lymph node imaging, 100 μL of the PEG-RITC-TaO_x solution was injected

Scheme 1. Schematic Illustration of the Synthesis and Surface Modification of TaO_x Nanoparticles, and Their Applications to X-ray CT Imaging

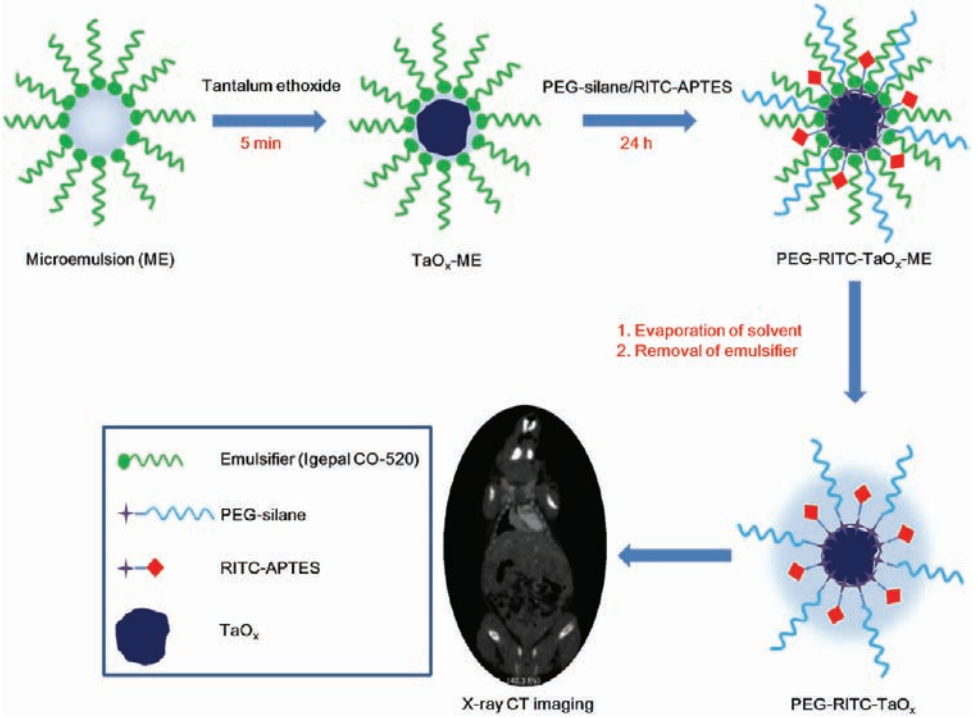

intradermally into the paws of rats, which were repeatedly imaged up to 2 h after injection. CT images were acquired using a Brilliance 64-slice CT Scanner (Philips Medical System). Imaging parameters were as follows: thickness, 0.1 mm; pitch, 0.648; 120 kVp, 192 mA; field of view, 108 × 108; matrix, 1024 × 1024 pixels; gantry rotation time, 0.75 s; table speed, 16.7 mm/s. Thin-section axial images were reformed to coronal images through a computational technique referred to as multiplanar-reconstruction (MPR). The three-dimensional (3-D) reconstructed images were obtained using OsiriX (version 3.8.1; 32 bit; OsiriX foundation, Geneva).

In Vitro and In Vivo Fluorescence Imaging. In vitro and in vivo fluorescence images were acquired using a fluorescence imaging system at an excitation wavelength of 550 nm (Kodak IS4000MM pro, U.S.).

RESULTS AND DISCUSSION

The overall synthetic process of the TaO_x nanoparticles was adopted from the microemulsion synthesis of silica nanoparticles with some modifications (Scheme 1).[12] We used 75 mM NaOH solution as a base catalyst for the sol−gel reaction of tantalum(V) ethoxide instead of typical ammonia catalyst used in silica sol−gel reactions because the reaction rate of tantalum(V) ethoxide is much faster than that of TEOS and ammonia catalyst would lead to uncontrolled agglomeration of nanoparticles. After emulsification of a mixture composed of cyclohexane, ethanol, NaOH, and Igepal CO-520 surfactant, tantalum(V) ethoxide was added to the emulsion. Controlled sol−gel reaction in the reverse micelles at room temperature led to the formation of uniform nanoparticles within 5 min. The transmission electron microscopy (TEM) image of the as-prepared TaO_x nanoparticles in micelles (TaO_x-ME) showed that the size distribution of the nanoparticles was very narrow ($\sigma_r \leq 5\%$) (Figure 1a). X-ray photoelectron spectroscopy (XPS) data (Figure S1a in the Supporting Information) revealed that the nanoparticles are composed of tantalum suboxides (TaO_x, $x \approx 1$).[13] X-ray diffraction (XRD) and electron diffraction (ED) patterns showed that the nanoparticles were amorphous (Figures S1b,c in the Supporting Information). The size of the nanoparticles could be controlled in the range of 5−15 nm by varying the amount of ethanol (Figure 2).[14] The increased amount of ethanol seems to have resulted in a decrease of hydrolysis rate of tantalum ethoxide, which eventually led to production of large nanoparticles.[15]

Surface modification of the TaO_x nanoparticles was directly performed using various silane agents without purification after the synthesis of the TaO_x-ME. Because the surface of unmodified TaO_x nanoparticles is acidic and reactive toward condensation reactions, TaO_x nanoparticles would be irreversibly aggregated without additional stabilization. Among the various silane moieties, PEG-silane and dye-conjugated silane were chosen because they are representative biocompatible polymer and fluorescent probe, respectively. Simple silica sol−gel reaction between the hydroxyl groups of the TaO_x-ME and silane reagents led to the formation of functionalized-silica-coated TaO_x nanoparticles, which can be applied to multifunctional imaging platforms with multiple modality and/or targeting/therapeutic functions.[16]

Long-circulating nanoparticles are required for effective X-ray CT imaging, such as angiography and tissue specific imaging. To avoid rapid clearance from the bloodstream by reticuloendothelial system (RES) uptake, PEG-silane was immobilized on the TaO_x nanoparticles as an antifouling agent. For fluorescence imaging, rhodamine B isothiocyanate (RITC)-conjugated aminopropyltriethoxysilane (APTES) was attached to the TaO_x nanoparticles. RITC-conjugated-APTES and PEG-silane were simultaneously immobilized on the TaO_x-ME to produce tantalum

dx.doi.org/10.1021/ja200120k | J. Am. Chem. Soc. 2011, 133, 5508–5515

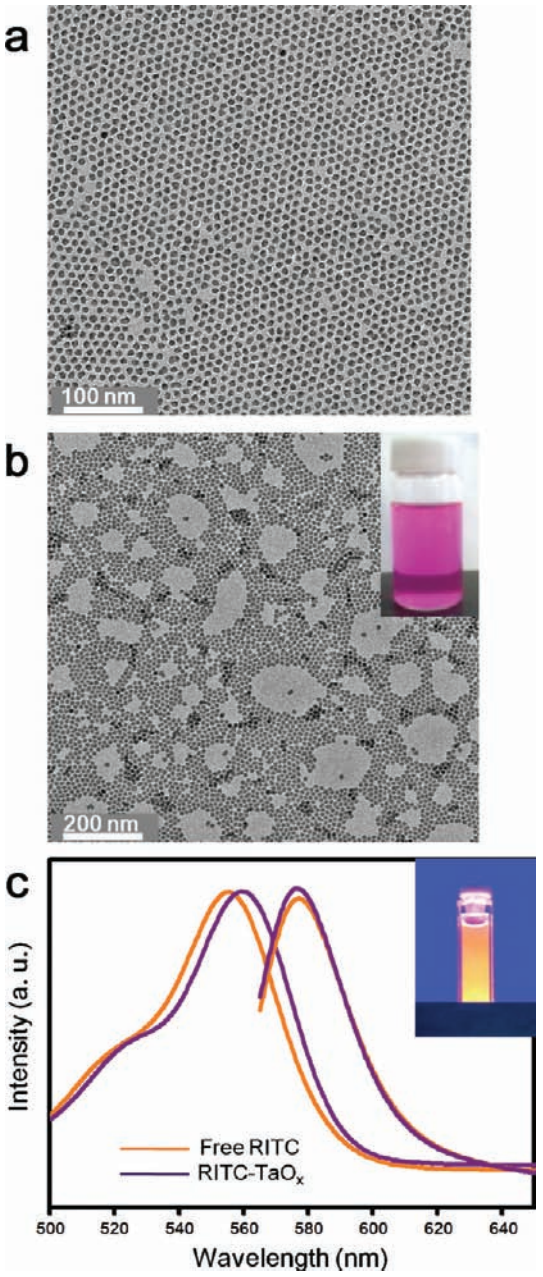

Figure 1. (a) TEM image of as-prepared TaO_x nanoparticles in microemulsion, and (b) TEM image of PEG-RITC-TaO_x dispersed in water (inset: photograph of the aqueous dispersion of nanoparticles). (c) Absorbance and fluorescence spectra of PEG-RITC-TaO_x and free RITC in PBS solution. Optical densities were equalized to match the number of RITC molecules in both samples (λ_{ex} = 520 nm, inset: photographic image of the fluorescent nanoparticles in PBS solution excited with UV light).

oxide nanoparticles conjugated with both PEG and RITC, designated as PEG-RITC-TaO_x. The TEM image of PEG-RITC-TaO_x (Figure 1b) showed that the nanoparticles were well dispersed in water, whereas no agglomerated nanoparticles were observed. ^{29}Si NMR spectroscopy revealed a single band corresponding to T^2 bonding sites centered at $\delta \approx -55$ ppm, demonstrating that PEG-silane formed on the surface of the nanoparticles while no separate silica particle formed (Figure S2a in the Supporting Information).[17] As shown in the inset of Figure 1c,

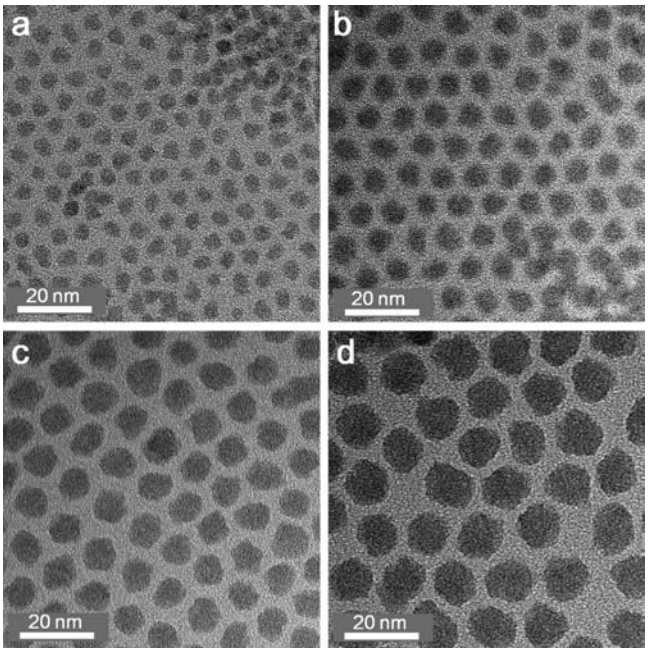

Figure 2. Size-controlled synthesis of TaO_x nanoparticles. (a–d) TEM images of 6, 9, 13, and 15 nm-sized TaO_x nanoparticles in microemulsion.

PEG-RITC-TaO_x was transparent, which is advantageous for fluorescence imaging. RITC-conjugated TaO_x exhibited comparable photoluminescence to free RITC (Figure 1c), indicating that the conjugated dyes were stable and that their fluorescence was preserved even after the conjugation reaction. The hydrodynamic diameter (HD) of the particles as measured by dynamic light scattering (DLS) was approximately 19 nm, demonstrating that no aggregation occurred (Figure S2b in the Supporting Information), which matched very well with the TEM data. The XPS spectrum of PEG-RITC-TaO_x was similar to that of the TaO_x nanoparticles in microemulsion, and Ta $4f_{7/2}$ (red) and Ta $4f_{5/2}$ (blue) peaks at 26 and 24.1 were in good agreement with the positions of peaks associated with TaO in the literature (Figure S3 in the Supporting Information).[13] The current synthetic process is relatively easy to scale up. For example, when we ran the reaction with 50 times as much material, as much as 6.4 g of PEG-RITC-TaO_x was obtained in a single batch (Figure S4).

X-ray CT phantom images were acquired using various concentrations of PEG-RITC-TaO_x dispersed in deionized water. The CT numbers, called Hounsfield units (HU), increased linearly as the concentration of the nanoparticles increased (Figure 3a). Although the contrast enhancement of Ta atom is slightly smaller than that of Au atom in diagnostic X-ray spectra (4.302 and 5.158 cm^2/g, respectively, at 100 keV), the measured HU values of the TaO_x nanoparticles were much higher than those of current iodine-based X-ray contrast agents.[6a,7a,10] MTT assay revealed that cell viability was not hindered by PEG-RITC-TaO_x up to a concentration of 2.4 mg of Ta/mL (Figure 3b), which is an extremely high concentration. Cellular X-ray CT and fluorescence imaging were conducted to demonstrate dose-dependent uptake and in vitro multimodal imaging capability of PEG-RITC-TaO_x. Cellular uptake was investigated by incubating murine macrophage cells (RAW264.7) with different concentrations of nanoparticles in serum-containing media. The confocal laser scanning microscopy (CLSM) images in Figure 3c revealed

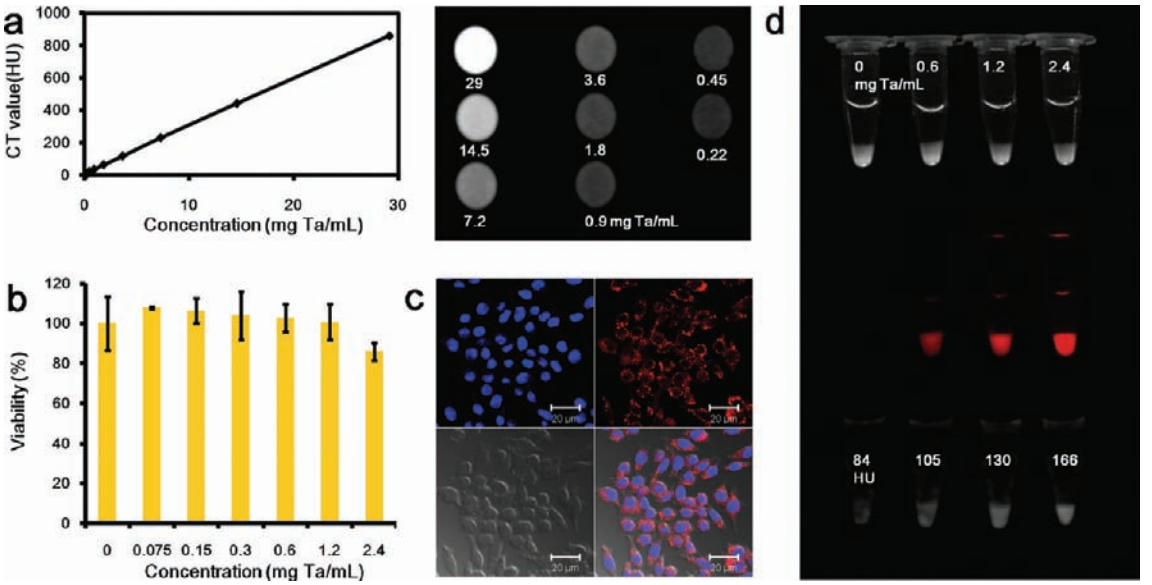

Figure 3. In vitro characterization of PEG-RITC-TaO_x. (a) HU measurements (left) and phantom CT image (right) of PEG-RITC-TaO_x in water. (b) RAW264.7 cells (murine macrophages) were cultured with the nanoparticles of various concentrations. Cytotoxicity of the nanoparticles was determined by MTT assay. (c) CLSM images of RAW264.7 cells incubated with PEG-RITC-TaO_x for 24 h (scale bar: 20 μm). The nuclei were stained blue with 4′-6-diamidino-2-phenylindole (DAPI). (d) Cellular imaging results of RAW264.7 cells incubated with various concentrations of PEG-RITC-TaO_x. Bright field image (top), fluorescence image (λ_{ex} = 550 nm) (middle), and X-ray CT image of cell phantom (numbers indicate CT values in HU) (bottom).

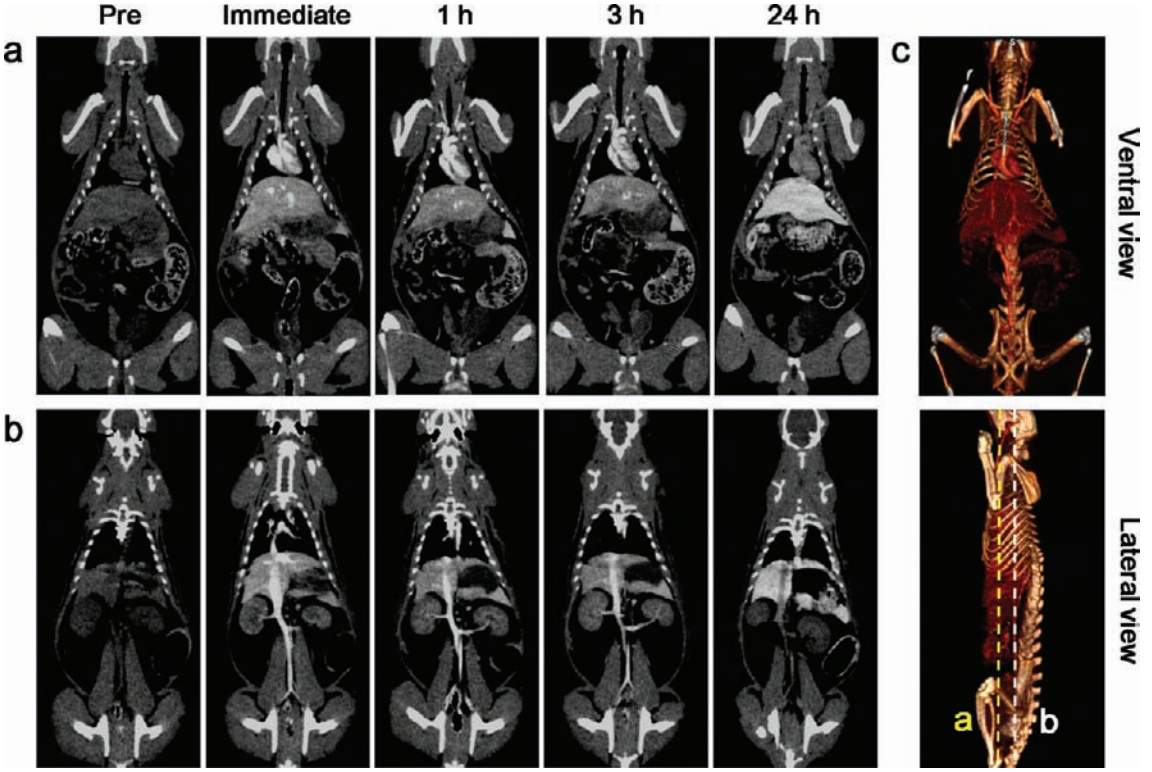

Figure 4. In vivo X-ray CT imaging. (a,b) Serial CT coronal views of a rat following injection of 1 mL of PEG-RITC-TaO_x solution (840 mg/kg) into the tail vein. (a) Heart and liver (coronal view cut along the yellow dotted line in (c)). (b) Spleen, kidney, and inferior vena cava (coronal view cut along the white dotted line in (c)). (c) 3D-renderings of in vivo CT images reveal the ventral (top) and lateral (bottom) sides of the heart and great vessels. The images were obtained immediately after injection.

that the nanoparticles were taken up by RAW264.7 cells via endocytosis. Fluorescence images of the cells after uptake of the nanoparticles show that the red luminescence became more intense and that HU values increased as the concentration increased

dx.doi.org/10.1021/ja200120k |J. Am. Chem. Soc. 2011, 133, 5508–5515

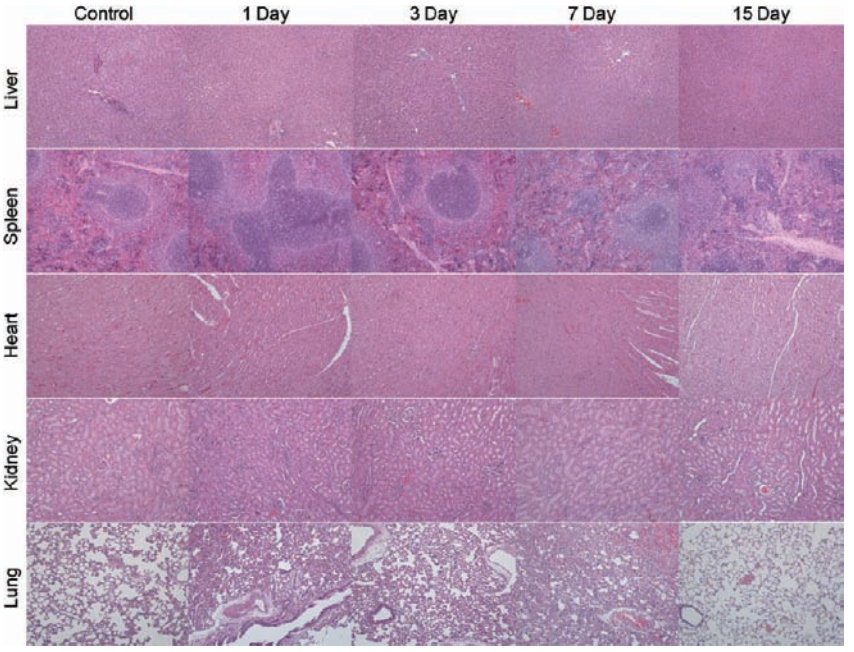

Figure 5. Time course of histological changes in the liver, spleen, heart, kidney, and lung of rats that received single intravenous injection of 1 mL of either PBS (control) or PEG-RITC-TaO_x (840 mg/kg dose in PBS) followed by dissection at the indicated times. Sections were stained with H&E and observed under a light microscope at 100× magnification.

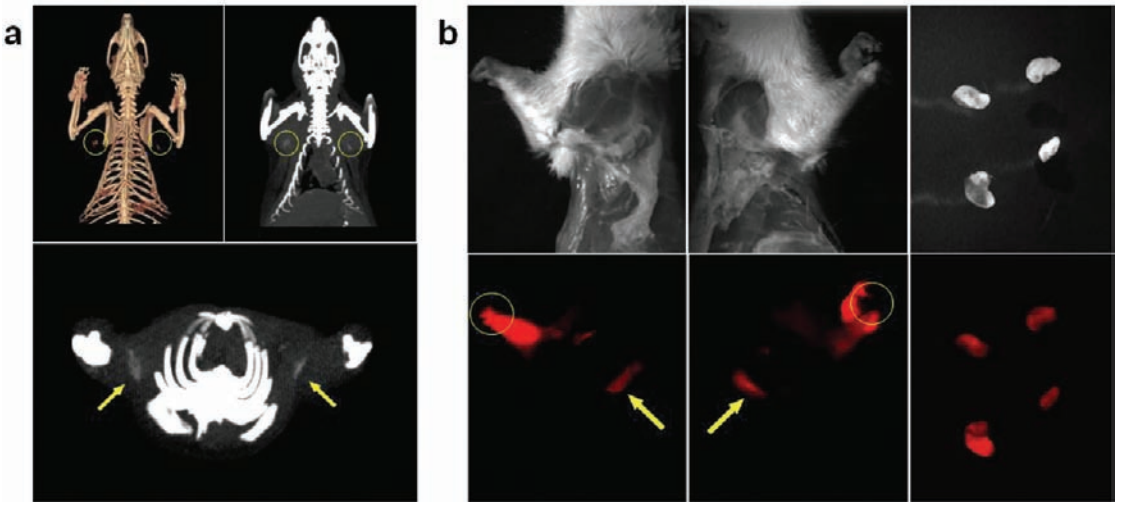

Figure 6. Sentinel lymph node mapping and resection. (a) In vivo CT volume-rendered (upper left) and maximum intensity projections (MIP) images (upper right and lower panels) of the sentinel lymph node of the rat were obtained 2 h after intradermal injection of 100 μL of PEG-RITC-TaO_x solution (210 mg/mL) in both paws. The yellow circles and arrows indicate the locations of the lymph nodes. (b) White light photographs (upper panels) and fluorescence images (lower panels) of the rat injected intradermally with 100 μL of PEG-RITC-TaO_x solution in both paws. Lateral views of the rat 2 h after injection show highly intense red emission from the lymph node and injected part (left and middle). Arrows and circles indicate the putative axillary sentinel lymph nodes and injection point, respectively. Sentinel lymph nodes of the two rats dissected by bimodal image-guided surgery (right).

(Figure 3d). These fluorescence and X-ray CT results demonstrated in vitro bimodal imaging capability as well as dose-dependent uptake of the TaO_x nanoparticles by mammalian cells.

To perform in vivo X-ray CT imaging, PEG-RITC-TaO_x (840 mg/kg) was injected intravenously into the tail vein of a rat. Distribution of the particles was tracked by X-ray CT imaging before injection as well as immediately, 5 min, 30 min, 1 h, 2 h, 3 h, and 24 h after injection (Figure 4a,b). Once the nanoparticles were injected, the vessels were preferentially enhanced, enabling spatially described, volume-rendered images of the blood pool (Figure 4c and Supporting Information movie 1). The enhancement continued for over 3 h, indicating long circulation of the particles. The nanoparticles were eventually accumulated by macrophages in the spleen and liver. The HU values of the blood vessels and heart reached maximum values immediately after injection and then decrease slowly, whereas the HU values of the liver and spleen gradually increased (Table S1 in the Supporting Information).

dx.doi.org/10.1021/ja200120k |*J. Am. Chem. Soc.* 2011, 133, 5508–5515

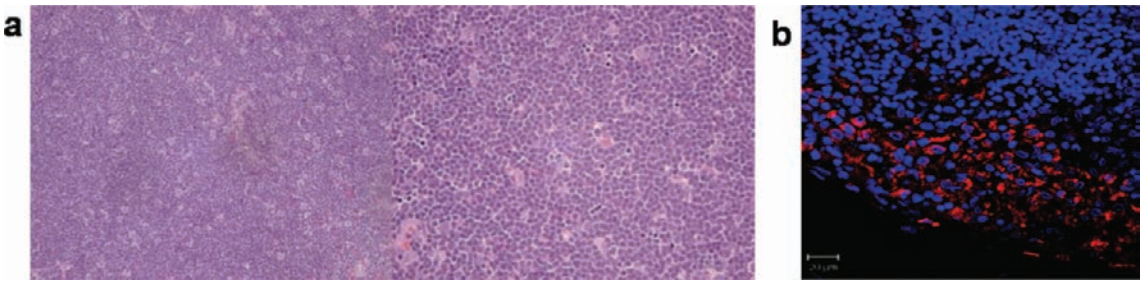

Figure 7. (a) Histological section of lymph node sample dissected by the bimodal image-guided surgery. Sections were stained with H&E and observed under a light microscope at 100× (left) and 400× (right) magnification. (b) Confocal microscopy image of the dissected lymph node stained blue with 4′-6-diamidino-2-phenylindole (DAPI) showing existence of PEG-RITC-TaO_x emitting red fluorescence.

After 24 h of CT imaging, the rat was sacrificed, and the biodistribution of PEG-RITC-TaO_x was visualized by fluorescence imaging of the dissected organs. CLSM images of the samples showed that most of the nanoparticles were found in the liver and spleen (Figure S5 in the Supporting Information). To determine whether PEG-RITC-TaO_x caused any harmful effects or any diseases in these organs, long-term toxicity of the nanoparticles was investigated by monitoring histological changes in several organs, including the liver, spleen, heart, kidney, and lung, for more than 2 weeks. Rats were dissected at 1 day, 3 day, 7 day, and 15 day after the injection of single dose (840 mg/kg) of PEG-RITC-TaO_x. Hematoxylin and eosin (H&E) stains of their organs showed no evidence of adverse effect of the nanoparticles (Figure 5). Serum levels of alanine aminotransferase (ALT) and aspartate aminotransferase (AST) were also measured over time to determine the effect on liver function. The single dose injection induced a transient increase of the serum level, which declined rapidly and returned to normal at day 3 (Figure S6 in the Supporting Information).[18] These results demonstrate that tantalum oxide nanoparticles exhibit little toxicity on liver as well as other organs.

Sentinel lymph node mapping is very important for the precise determination of tumor metastasis.[19] By precisely mapping the lymph nodes, unnecessary dissection from surgery can be avoided. To deliver the contrast agent to sentinel lymph nodes, 100 μL of PEG-RITC-TaO_x solution was intradermally injected into the rats' paws. Two hours following injection, the locations of the lymph nodes were determined by X-ray contrast enhancement (Figure 6a and Supporting Information movie 2). To investigate whether or not the resection of lymph nodes can be assisted by bimodal imaging, the locations of the lymph nodes were first determined using the volume-rendered CT images. Once a site was located, the area of the lymph nodes to be dissected was specified using fluorescence imaging during the operation, followed by successful extraction (Figure 6b). In the dissected lymph nodes, nanoparticles were found by fluorescence imaging, but no histological changes were observed by H&E staining (Figure 7).

CONCLUSIONS

Gram-scale synthesis of uniform-sized TaO_x nanoparticles was achieved using a simple microemulsion method. One-pot surface modification using various silane derivatives was successfully integrated to the microemulsion synthetic system, providing PEGylated and dye-immobilized TaO_x nanoparticles with antifouling and multimodal capabilities. In vivo X-ray CT imaging using RITC-conjugated and PEGylated TaO_x nanoparticles resulted in bright and well-resolved CT images with long circulation time. Time-course of histological studies and liver toxicity test revealed no adverse effect of the nanoparticles, possibly due to their bioinertness. Bimodal image-guided surgery using the particles was also advantageous in the resection of lymph nodes. These results clearly demonstrate that TaO_x nanoparticles can be used for various multifunctional medical applications. In terms of practical clinical applications, tantalum oxide nanoparticles have potentials for angiography as well as RES-targeted imaging to improve the detection of metastases in the liver and lymph nodes.[19]

ASSOCIATED CONTENT

Supporting Information. XPS, ED, and XRD data of 9 nm TaO_x nanoparticles, ^{29}Si CP MAS NMR spectrum and DLS data of PEG silane immobilized TaO_x nanoparticles, TEM image of 9 nm-sized PEG-RITC-TaO_x nanoparticles synthesized in large scale, HU values of the organs after the intravenous injection, biodistribution of PEG-RITC-TaO_x by the measurement of fluorescence, changes in serum liver enzyme levels as a function of time, and complete ref 6g. This material is available free of charge via the Internet at http://pubs.acs.org.

AUTHOR INFORMATION

Corresponding Author

thyeon@snu.ac.kr; choiseunghong@gmail.com

Author Contributions

‖These authors contributed equally.

ACKNOWLEDGMENT

We gratefully acknowledge financial support by the Korean Ministry of Education, Science, and Technology through the National Creative Research Initiative (R16-2002-003-01001-0), Strategic Research (2010-0029138), and World Class University (R31-10013) Programs of the National Research Foundation (NRF) of Korea.

REFERENCES

(1) (a) Alivisatos, A. P. *Nat. Biotechnol.* **2004**, *22*, 47. (b) Rosi, N. L.; Mirkin, C. A. *Chem. Rev.* **2005**, *105*, 1547. (c) Michalet, X.; Pinaud, F. F.; Bentolila, L. A.; Tsay, J. M.; Doose, S.; Li, J. J.; Sundaresan, G.; Wu, A. M.; Gambhir, S. S.; Weiss, S. *Science* **2005**, *307*, 538. (d) Weissleder, R.; Pittet, M. J. *Nature* **2008**, *452*, 580. (e) Selvan, S. T.; Patra, P. K.; Ang, C. Y.; Ying, J. Y. *Angew. Chem., Int. Ed.* **2007**, *46*, 2448. (f) Klostranec, J. M.; Chan, W. C. W. *Adv. Mater.* **2006**, *18*, 1953. (g) Kim, J.-W.;

Galanzha, E. I.; Shashkov, E. V.; Moon, H.-M.; Zharov, V. P. *Nat. Nanotechnol.* **2009**, *4*, 688. (h) Lee, S.-M.; Park, H.; Yoo, K.-H. *Adv. Mater.* **2010**, *22*, 4049.

(2) (a) Barnett, B. P.; Arepally, A.; Karmarkar, P. V.; Qian, D.; Gilson, W. D.; Walczak, P.; Howland, V.; Lawler, L.; Lauzon, C.; Stuber, M.; Kraitchman, D. L.; Bulte, J. W. M. *Nat. Med.* **2007**, *13*, 986. (b) Choi, H. S.; Liu, W.; Liu, F.; Nasr, K.; Misra, P.; Bawendi, M. G.; Frangioni, J. V. *Nat. Nanotechnol.* **2010**, *5*, 42. (c) Kumar, R.; Roy, I.; Ohulchanskky, T. Y.; Vathy, L. A.; Bergey, E. J.; Sajjad, M.; Prasad, P. N. *ACS Nano* **2010**, *4*, 699. (d) Perrault, S. D.; Walkey, C.; Jennings, T.; Fischer, H. C.; Chan, W. C. W. *Nano Lett.* **2009**, *9*, 1909.

(3) (a) Larson, D. R.; Zipfel, W. R.; Williams, R. M.; Clark, S. W.; Bruchez, M. P.; Wise, F. W.; Webb, W. W. *Science* **2003**, *300*, 1434. (b) Medintz, I. L.; Uyeda, H. T.; Goldman, E. R.; Mattoussi, H. *Nat. Mater.* **2005**, *4*, 435. (c) Bakalova, R.; Zhelev, Z.; Aoki, I.; Kanno, I. *Nat. Photon.* **2007**, *1*, 487. (d) Bruchez, M., Jr.; Moronne, M.; Gin, P.; Weiss, S.; Alivisatos, A. P. *Science* **1998**, *281*, 2013.

(4) (a) Bulte, J. W. M.; Kraitchman, D. L. *NMR Biomed.* **2004**, *17*, 484. (b) Laurent, S.; Forge, D.; Port, M.; Roch, A.; Robic, C.; Vander Elst, L.; Muller, R. N. *Chem. Rev.* **2008**, *108*, 2064. (c) Lin, W.; Hyeon, T.; Lanza, G. M.; Zhang, M.; Meade, T. J. *MRS Bull.* **2009**, *34*, 441. (d) Jun, Y.-W.; Lee, J.-H.; Cheon, J. *Angew. Chem., Int. Ed.* **2008**, *47*, 5122. (e) Na, H. B.; Hyeon, T. *J. Mater. Chem.* **2009**, *19*, 6267. (f) Na, H. B.; Song, I. C.; Hyeon, T. *Adv. Mater.* **2009**, *21*, 2133. (g) Jun, Y.-W.; Huh, Y.-M.; Choi, J.-S.; Lee, J.-H.; Song, H.-T.; Kim, S.; Yoon, S.; Kim, K.-S.; Shin, J.-S.; Suh, J.-S.; Cheon, J. *J. Am. Chem. Soc.* **2005**, *127*, 5732. (h) Lewin, M.; Carlesso, N.; Tung, C.-H.; Tang, X.-W.; Cory, D.; Scadden, D. T.; Weissleder, R. *Nat. Biotechnol.* **2000**, *18*, 410. (i) Lee, J.-H.; Huh, Y.-M.; Jun, Y.-W.; Seo, J.-W.; Jang, J.-T.; Song, H.-T.; Kim, S.; Cho, E.-J.; Yoon, H.-G.; Suh, J.-S.; Cheon, J. *Nat. Med.* **2007**, *13*, 95. (j) Gao, J.; Liang, G.; Cheung, J. S.; Pan, Y.; Kuang, Y.; Zhao, B. Z.; Zhang, X.; Wu, E. X.; Xu, B. *J. Am. Chem. Soc.* **2008**, *130*, 11828.

(5) Schwenzer, N. F.; Springer, F.; Schraml, C.; Stefan, N.; Machann, J.; Schick, F. *J. Hepatol.* **2009**, *51*, 433.

(6) (a) Yu, S.; Watson, A. D. *Chem. Rev.* **1999**, *99*, 2353. (b) Frangioni, J. V. *Nat. Biotechnol.* **2006**, *24*, 909. (c) Gao, X.; Cui, Y.; Levenson, R. M.; Chung, L. W. K.; Nie, S. *Nat. Biotechnol.* **2004**, *22*, 969. (d) Xie, J.; Chen, K.; Lee, H.-Y.; Xu, C.; Hsu, A. R.; Peng, S.; Chen, X.; Sun, S. *J. Am. Chem. Soc.* **2008**, *130*, 7542. (e) Santra, S.; Bagwe, R. P.; Dutta, D.; Stanley, J. T.; Walter, G. A.; Tan, W.; Moudgil, B. M.; Mericle, R. A. *Adv. Mater.* **2005**, *17*, 2165. (f) Prencipe, G.; Tabakman, S. M.; Welsher, K.; Liu, Z.; Goodwin, A. P.; Zhang, L.; Henry, J.; Dai, H. *J. Am. Chem. Soc.* **2009**, *131*, 4783. (g) Sun, I.-C.; et al. *Chem.-Eur. J.* **2009**, *15*, 13341.

(7) (a) Kim, D.; Park, S.; Lee, J. H.; Jeong, Y. Y.; Jon, S. Y. *J. Am. Chem. Soc.* **2007**, *129*, 7661. (b) Rabin, O.; Perez, J. M.; Grimm, J.; Wojtkiewicz, G.; Weissleder, R. *Nat. Mater.* **2006**, *5*, 118. (c) Popovtzer, R.; Agrawal, A.; Kotov, N. A.; Popovtzer, A.; Balter, J.; Carey, T. E.; Kopelman, R. *Nano Lett.* **2008**, *8*, 4593. (d) Kattumuri, V.; Katti, K.; Bhaskaran, S.; Boote, E. J.; Casteel, S. W.; Fent, G. M.; Roberston, D. J.; Chandrasekhar, M.; Kannan, R.; Katti, K. V. *Small* **2007**, *3*, 333.

(8) (a) deKrafft, K. E.; Xie, Z.; Cao, G.; Tran, S.; Ma, L.; Zhou, O. Z.; Lin, W. *Angew. Chem., Int. Ed.* **2009**, *48*, 9901. (b) Pan, D.; Williams, T. A.; Senpan, A.; Allen, J. S.; Scott, M. J.; Gaffney, P. J.; Wickline, S. A.; Lanza, G. M. *J. Am. Chem. Soc.* **2009**, *131*, 15522. (c) Hyafil, F.; Cornily, J.-C.; Feig, J. E.; Gordon, R.; Vucic, E.; Amirbekian, V.; Fisher, E. A.; Fuster, V.; Fledman, L. J.; Fayad, Z. A. *Nat. Med.* **2007**, *13*, 636. (d) Alric, C.; Taleb, J.; Duc, G. L.; Mandon, C.; Billotey, C.; Meur-Herland, A. L.; Brochard, T.; Vocanson, F.; Janier, M.; Perriat, P.; Roux, S.; Tillement, O. *J. Am. Chem. Soc.* **2008**, *130*, 5908. (e) Bhang, S. H.; Won, N.; Lee, T.-J.; Jin, H.; Nam, J.; Park, J.; Chung, H.; Park, H.-S.; Sung, Y.-E.; Hahn, S. K.; Kim, B.-S.; Kim, S. *ACS Nano* **2009**, *3*, 1389. (f) Gao, J.; Zhang, B.; Gao, Y.; Pan, Y.; Zhang, X.; Xu, B. *J. Am. Chem. Soc.* **2007**, *129*, 11928. (g) Xu, C.; Xie, J.; Ho, D.; Wang, C.; Kohler, N.; Walsh, E. G.; Morgan, J. R.; Chin, Y. E.; Sun, S. *Angew. Chem., Int. Ed.* **2007**, *47*, 173. (h) Cheon, J.; Lee, J.-H. *Acc. Chem. Res.* **2008**, *41*, 1630.

(9) (a) Black, J. *Clin. Mater.* **1994**, *16*, 167. (b) Matsuno, H.; Yokoyama, A.; Watari, F.; Uo, M.; Kawasaki, T. *Biomaterials* **2001**, *22*, 1253. (c) Kato, H.; Nakamura, T.; Nishiguchi, S.; Matsusue, Y.; Kobayashi, M.; Miyazaki, T.; Kim, H.-M.; Kokubo, T. *J. Biomed. Mater. Res.* **2000**, *53*, 28. (d) Sharma, C. P.; Paul, W. *J. Biomed. Mater. Res.* **1992**, *26*, 1179. (e) Miller, A. C.; Fuciarelli, A. F.; Jackson, W. E.; Ejnik, E. J.; Emond, C.; Strocko, S.; Hogan, J.; Page, N.; Pellmar, T. *Mutagenesis* **1998**, *13*, 643. (f) Johnson, P. F.; Bernstein, J. J.; Hunter, G.; Dawson, W. W.; Hench, L. L. *J. Biomed. Mater. Res.* **1977**, *11*, 637. (g) Zitter, H.; Plenk, H., Jr. *J. Biomed. Mater. Res.* **1987**, *21*, 881. (h) Chen, J. Y.; Leng, Y. X.; Tian, X. B.; Wang, L. P.; Huang, N.; Chu, P. K.; Yang, P. *Biomaterials* **2002**, *23*, 2545. (i) Findlay, D. M.; Welldon, K.; Atkins, G. J.; Howie, D. W.; Zannettino, A. C. W.; Bobyn, D. *Biomaterials* **2004**, *25*, 2215.

(10) Bonitatibus, P. J., Jr.; Torres, A. S.; Goddard, G. D.; FitzGerald, P. F.; Kulkarni, A. M. *Chem. Commun.* **2010**, *46*, 8956.

(11) (a) Kim, S.; Lim, Y. T.; Soltesz, E. G.; Grand, A. M. D.; Lee, J.; Nakayama, A.; Parker, J. A.; Mihaljevic, T.; Laurence, R. G.; Dor, D. M.; Cohn, L. H.; Bawendi, M. G.; Frangioni, J. V. *Nat. Biotechnol.* **2004**, *22*, 93. (b) Kobayashi, H.; Hama, Y.; Koyama, Y.; Barrett, T.; Regino, C. A. S.; Urano, Y.; Choyke, P. L. *Nano Lett.* **2007**, *6*, 1711.

(12) (a) Chang, C.; Fogler, S. *Langmuir* **1997**, *13*, 3295. (b) Arriagada, F. J.; Osseo-asare, K. *J. Colloid Interface Sci.* **1999**, *211*, 210.

(13) Lecuyer, S.; Quemerais, A.; Jezequel, G. *Surf. Interface Anal.* **1992**, *18*, 257.

(14) (a) Xu, C.; Tung, G. A.; Sun, S. *Chem. Mater.* **2008**, *20*, 4167. (b) Burns, A. A.; Vider, J.; Ow, H.; Herz, E.; Penate-Medina, O.; Baumgart, M.; Larson, S. M.; Wiesner, U.; Bradbury, M. *Nano Lett.* **2009**, *9*, 442. (c) Chithrani, B. D.; Chan, W. C. W. *Nano Lett.* **2007**, *7*, 1542.

(15) Ogihara, T.; Ikemoto, T.; Mizutani, N.; Kato, M. *J. Mater. Sci.* **1986**, *21*, 2771.

(16) (a) Tan, W.; Wang, K.; He, X.; Zhao, X. J.; Drake, T.; Wang, L.; Bagwe, R. P. *Med. Res. Rev.* **2004**, *24*, 621. (b) Ow, H.; Larson, D. R.; Srivastava, M.; Baird, B. A.; Webb, W. W.; Wiesner, U. *Nano Lett.* **2005**, *5*, 113. (c) Burns, A.; Ow, H.; Wiesner, U. *Chem. Soc. Rev.* **2006**, *35*, 1028. (d) Kim, J.; Kim, H. S.; Lee, N.; Kim, T.; Kim, H.; Yu, T.; Song, I. C.; Moon, W. K.; Hyeon, T. *Angew. Chem., Int. Ed.* **2008**, *47*, 8438. (e) Piao, Y.; Burns, A.; Kim, J.; Wiesner, U.; Hyeon, T. *Adv. Funct. Mater.* **2008**, *18*, 3745. (f) Kim, J.; Piao, Y.; Hyeon, T. *Chem. Soc. Rev.* **2009**, *38*, 372. (g) Lee, J. E.; Lee, N.; Kim, H.; Kim, J.; Choi, S. H.; Kim, J. H.; Kim, T.; Song, I. C.; Park, S. P.; Moon, W. K.; Hyeon, T. *J. Am. Chem. Soc.* **2009**, *132*, 552.

(17) Schulz, H.; Pratsinis, S. E.; Rüegger, H.; Zimmermann, J.; Klapdohr, S.; Salz, U. *Colloids Surf., A* **2008**, *315*, 79.

(18) (a) Jain, T. K.; Reddy, M. K.; Morales, M. A.; Leslie-Pelecky, D. L.; Labhasetwar, V. *Mol. Pharmaceutics* **2008**, *5*, 316. (b) Hainfeld, J. F.; Slatkin, D. N.; Focella, T. M.; Smilowitz, H. M. *Br. J. Radiol.* **2006**, *79*, 248.

(19) Harisinghani, M. G.; Barentsz, J.; Hahn, P. F.; Deserno, W. M.; Tabatabaei, S.; van de Kaa, C. H.; de la Rosette, J.; Weissleder, R. *N. Engl. J. Med.* **2003**, *348*, 2491.